Discerning aggregation in homogeneous ensembles: A general description of photon counting spectroscopy in diffusing systems

Hai-Cang Ren,[1] Noel L. Goddard,[2] Grégoire Altan-Bonnet,[2,*] and Albert Libchaber[2]
[1]*Laboratory for Theoretical Physics, The Rockefeller University, New York, New York 10021, USA*
[2]*Center for Studies in Physics and Biology, The Rockefeller University, New York, New York 10021, USA*
(Received 3 January 2003; published 27 May 2004)

In order to discern aggregation in solution, we present a quantum mechanical analog of the photon statistics from fluorescent molecules diffusing through a focused beam. A generating functional is developed to fully describe the experimental physical system as well as the statistics. Histograms of the measured time delay between photon counts are fit by an analytical solution describing the static as well as diffusing regimes. To determine empirical fitting parameters, fluorescence correlation spectroscopy is used in parallel to the photon counting. For expedient analysis, we find that the distribution's deviation from a single Poisson shows a difference between two single fluor monomers or a double fluor aggregate of the same total intensities. Initial studies were performed on fixed-state aggregates limited to dimerization. However preliminary results on reactive species suggest that the method can be used to characterize any aggregating system.

DOI: 10.1103/PhysRevE.69.051916 PACS number(s): 87.15.Kg, 34.50.−s, 32.50.+d

I. INTRODUCTION

Aggregation and cooperative binding are fundamental to biological function and regulation, but difficult to observe at the few molecule level. Recent advances in few molecule solution spectroscopy have been achieved by combining the comparatively large signals of fluorescence with recent technological advances in photon counting (e.g., low noise detectors). One powerful technique, fluorescence correlation spectroscopy (FCS), has enabled researchers to observe many small ensemble processes such as diffusion [1], molecular conformational dynamics [2], and reaction kinetics [3]. In FCS, fluctuations in fluorescence intensity are temporally correlated to reveal the time scale of the underlying fluctuation source. In the simplest case, this could be the diffusion time scale of a fluorescent molecule through a sampling volume. However, it is difficult to discern aggregation based on the diffusion time alone since the increase in diffusion time between a monomer and a dimer is weakly dependent on the increase in effective radius ($\propto\langle r^2\rangle^{1/2}$ for hard spheres) [4].

An alternative approach to FCS is the statistical analysis of the time series of emitted photons (number counting Fig. 1), since the number distribution of fluorophores in the detection volume at any given moment is different for species of different quantum yield or fluorophore number. This analysis, called photon number counting histogram analysis [5,6], was originally developed to detect the "brightness" per particle, but relied on the static (nondiffusing) limit. However in experiment, several factors potentially overshadow the specific brightness signature of a fluor, such as triplet states, bleaching, or quenching. We propose a method of analysis, the *time delay histogram*, to discern small differences in a species' fluorescence complemented by differences in diffusive behavior. The time delay histogram is constructed of the time between successive photon counts (Fig. 1). Unlike counting the number of events per time bin, this type of counting allows us to extract additional information about the diffusion. Conceptually, as more fluorinated monomers aggregate, the fluorophores sample the detection volume in bunches. This increases the chance of a large time interval between two successive emission photons and the large Δt tail of the time delay histogram has an increased frequency.

To extract the information on the structural change, we have developed a generating functional to unify different statistical aspects of the photon time series. This functional is modeled as a transition matrix element of a fictitious quantum mechanical system evolving in an imaginary time. Many well developed techniques in quantum mechanics are borrowed to derive analytical expressions for other experimental observables such as the autocorrelation function. Our approach is complementary to the description model proposed by Novikov and Boens [7] for the photon counting histogram. An extension of our functional can also be applied to modern multi channel techniques [8,9] as well as the incor-

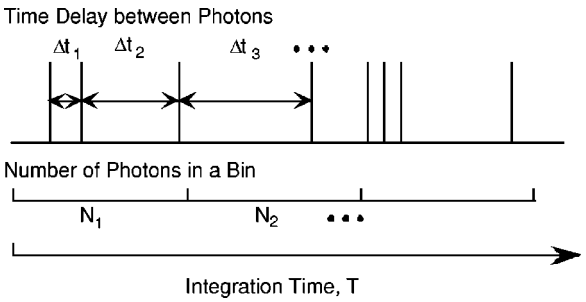

FIG. 1. Schematic of a photon counting trace. Traditional photon counting divides the total integration time into bins, counting the number that fall into each. We propose a different type of counting based on the time delay between two successive photon counts.

*Present address: Laboratory of Immunology, National Institute of Allergies and Infectious Diseases, National Institute of Health, Bethesda, MD 20892.

poration of secondary processes such as triplet states, bleaching, quenching, and chemical reaction kinetics.

Recently Kask and co-workers also proposed a method to extract the diffusion signature of a particle through fluorescence intensity multiple distribution analysis (FIMDA) [9]. In FIMDA, many histograms are constructed from the same time trace as the bin size is varied. In contrast, the time delay histogram we propose, contains the diffusion signature of the aggregate in a *single* histogram. At small time delays (less than the diffusion time through the collection volume) we are sensitive to the rate of photons emitted per object, and at greater delays, diffusion dominates the statistics. Finally, we offer a complementary technique to FIMDA using the Mandel Q parameter [12] to expediently extract diffusion information from number counting distributions. The power of this technique could be increased by greater photon collection capabilities, leading to better statistics and ultimately better discrimination, including higher moments, in the large delay limit.

To demonstrate the sensitivity of our analysis, we choose a case where the difference in diffusion times is negligible. A particularly difficult case is the discrimination of two monomers of identical fluorescence from a single dimer with the sum of their fluorescence. Although both have the same average rate of emitted photons, they sample the excitation beam profile differently as they diffuse (inhomogeneous intensity profile of a focused beam). For the experiment, a sequence of single-stranded DNA is specifically tagged with either one or two fluorophores per strand. The single-dyed strands will be considered "monomers" and the doubled tagged as "dimers." For all cases, we find good discrimination between samples of a given concentration of dimers versus that of twice the concentration of monomers, where both samples have the same average fluorescence.

II. OVERVIEW OF APPROACH

The time series of photon events may be described by the instantaneous fluorescence intensity

$$I(t) = \sum_{n}^{N} \delta_{\epsilon}(t - t_n), \tag{2.1}$$

where $t_1, t_2, \ldots, t_n, \ldots, t_N$ correspond to the tick marks of Fig. 1 with N total number of photons counted and ϵ is the detector resolution. $\delta_{\epsilon}(t-t_n)=1/\epsilon$ for $|t-t_n|<\epsilon$ and $\delta_{\epsilon}(t-t_n)=0$ otherwise. In the theoretical analysis of the subsequent sections, we shall take the limit $\epsilon \to 0$ so the instantaneous intensity becomes a random spike function. In the current literature statistical analysis tends to be limited to the average intensity,

$$I = \frac{1}{T}\int_0^T dt I(t), \tag{2.2}$$

and various types of correlation functions, the most familiar being the autocorrelation function

$$A(\tau) = \frac{1}{I^2}\left[\frac{1}{T}\int_0^{T-\tau} dt I(t) I(t+\tau) - I^2\right] - \delta_{\epsilon}(t) \tag{2.3}$$

for $T \gg \tau$, which decays with a characteristic time scale τ_D, the diffusion time through the collection volume. The subtraction of δ_{ϵ} permits $A(t)$ to vanish for all τ for a Poissonian histogram. Dividing the integration time into N_b bins of equal time interval τ, i.e., $T=N_b\tau$, the number of photon counts falling within the time bins are $m_1, m_2, \ldots, m_{N_b}$, and their moments

$$M_l = \frac{1}{N_b}\sum_{n=1}^{N_b} m_n^l \tag{2.4}$$

carry the structural information of the underlying fluorescence molecules. The quantity for comparison, called the Mandel's Q parameter, is defined as

$$\delta \equiv \frac{M_2 - M_1^2 - M_1}{M_1}, \tag{2.5}$$

where the first moment is defined by $M_1=I\tau$, etc. Although higher moments yield greater differentiation, we limit our analysis to the second moment due to the experimental collection capabilities ($\leqslant 2^{16}$ photons) of our system. The definition (2.3) and the relation $m_n=\int_{(n-1)\tau}^{n\tau} dt I(t)$ directly relates the Q parameter to the autocorrelation function,

$$\delta = \frac{2I}{\tau}\int_0^{\tau} ds(\tau - s)A(s). \tag{2.6}$$

Similar relations exist between higher order correlation functions and higher order binning moments.

Finally we describe the time delay histogram of the distribution of time intervals between two successive photon events, i.e., $\Delta t_1, \Delta t_2, \ldots$. For sufficiently large number of photon counts, a distribution function of Δt, $\rho(\Delta t)$, can be extracted, which has not been discussed in the literature. The theory of this function will be developed in Secs. IV and V will be compared with experimental result in Sec. VI.

III. EXPERIMENTAL MATERIALS AND METHODS

To create well-defined single or double fluor elements, short pieces of single-stranded DNA (ssDNA) were used as substrates. Either one or two fluorophores can be site-specifically coupled to each DNA oligomer (29 bases in length), dependent on the number of end-strand modifications (primary amino linker arms, Midland Certified Reagent Co.). Succidinmyl ester Rhodamine 6G (molecular probes) was coupled to the modified sites in the presence of DMF, and purified by gel filtration and reverse phases chromatography [high performance liquid chromatography (HPLC)].

The experimental setup (Fig. 2) is an inverted confocal microscopy arrangement. The sample is illuminated by the 514.5 nm line of a Ar+ laser (Lexel 85) focused through a 60× water immersion objective (numerical aperture 1.2, Olympus). Incident power was empirically optimized at 100 μW, so that the photon counts per object were at least 50 000 cps, while avoiding significant population of the trip-

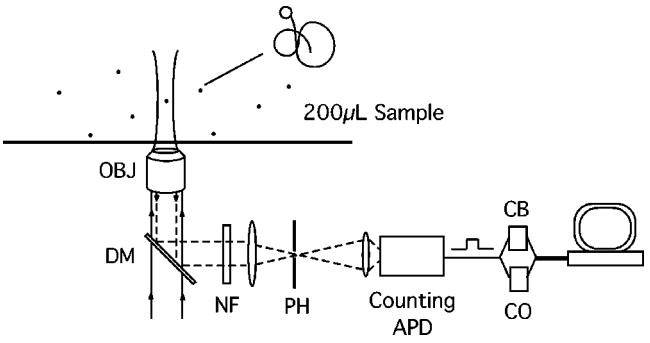

FIG. 2. Schematic of the photon counting setup. OBJ =objective, DM=dichroic mirror, NF=notch filter, PH =pinhole, APD=avalanche photodiode, CB=counting board, CO =correlator board.

let state or bleaching. Emitted photons are collected through the same objective, directed through a high-pass dichroic mirror (Omega Optical) and a notch filter (Kaiser Optical) to reduce collection of on-axis elastically scattered photons. The collection volume is further refined by focusing the light onto a 25 μm pinhole, eliminating off angle scattering as well as spatially defining the collection volume. The collection volume was empirically determined through the number of molecules measured through FCS as a function of increasing concentration. All FCS measurements were 10 min in duration using a ALV 5000 E board for data collection and in-house data analysis software for fitting. The overall detection efficiency of the setup is 3 %. Photons are detected by a counting avalanche photodiode (EG&G/Perkin Elmer), pulse width 25 ns, whose signal is processed by task specific counting board (NI-TIO 6602 National Instruments), controlled by LabVIEW. The period between each photon is measured by counting the number of external clock (4 MHz) pulses(source) between each photon pulse (gate). 2^{16} photons are collected for each trial. Data acquisition technology limited the total collection time to 1–2 s, depending on the incident intensity. After pulsing artifacts from the photodiodes were measured ~100 ns, with comparison to cross correlation of the same signal in two perpendicular detectors. Digital filtering was used to subtract the after pulsing noise from the final histogram statistics. DNA concentrations are ~nanomolars in PBS buffer such that only one monomer molecule at any time is within the collection volume.

Photon counting data are collected as fluorescent particles diffuse through the sample volume. When the particles are outside the volume they are dark and undetectable. As they enter the volume they are excited with a certain probability and emit a temporal pattern of photons that are detected by a counter. Given a long integration time, many particles diffuse through the volume producing temporal fluctuations in fluorescence. Whereas the autocorrelation function reveals the time scale of these fluorescence fluctuations, the probability distribution characterizes their amplitude.

IV. A MATHEMATICAL THEORY OF TIME DELAY HISTOGRAM

While there exist many papers in the literature on the mathematical properties of the photon event histogram [5,6], here we would like to provide a unified approach, which ties the experimental observables such as fluorescence intensity, autocorrelation, the binning moments, and time delay histogram to a probability generating functional.

A. General formulation

To begin, we divide the integration time T into $\mathcal{N}$ bins, each of interval ϵ, i.e., $T=\mathcal{N}\epsilon$. Each fluorescence diffusion process produces a histogram of photon counting, $\{m_1,\ldots,m_\mathcal{N}\}$, with m_l the number of photon events within the lth time bin and the corresponding fluorescence intensity given by

$$I_l = \frac{m_l}{\epsilon}. \tag{4.1}$$

Let $P_{m_1\cdots m_\mathcal{N}}$ stand for the probability of this particular time delay histogram. The generating function of this set of probabilities is defined as

$$\mathcal{G}(z_1,\ldots,z_\mathcal{N}) = \sum_{m_1,\ldots,m_\mathcal{N}} P_{m_1\cdots m_\mathcal{N}} z^{m_1}\cdots z^{m_\mathcal{N}}, \tag{4.2}$$

which is properly normalized, i.e., $\mathcal{G}(1,\ldots,1)=1$. In the limit $\epsilon\to 0$ (or, equivalently $\mathcal{N}\to\infty$ with a fixed T), the sequences $\{z_1,\ldots,z_\mathcal{N}\}$ and $\{I_1,\ldots,I_\mathcal{N}\}$ become two functions of t, $z(t)$ and $I(t)$, such that $z(l\epsilon)=z_l$ and $I(l\epsilon)=I_l$. In particular, as $\epsilon\to 0$, most m's vanish, few of them are equal to one, and the probability of $m_l>2$ becomes negligible. The function $I(t)$ approaches the random spike function introduced in the last section. In the same limit, the generating function (4.2) becomes a generating functional

$$\mathcal{G}[z(t)] = \lim_{\mathcal{N}\to\infty} \mathcal{G}(z_1,\ldots,z_\mathcal{N}). \tag{4.3}$$

An important set of observables are various correlation functions given by the functional derivatives of $\mathcal{G}$ with respect to $z(t)$ at $z(t)=1$, i.e.,

$$C_n(t_1,\ldots,t_n) = \frac{\delta}{\delta z(t_1)}\cdots\frac{\delta}{\delta z(t_n)}\ln \mathcal{G}[z(t)]\big|_{z(t)=1}. \tag{4.4}$$

The function $C_1(t)$ is nothing but the ensemble average of the instantaneous fluorescence intensity at the moment t,

$$\langle I(t)\rangle = C_1(t), \tag{4.5}$$

the coefficient $C_2(t_1,t_2)$ is related to the autocorrelation function between t_1 and t_2 via

$$A(t_1,t_2) = \frac{C_2(t_1,t_2)}{C_1(t_1)C_1(t_2)}, \tag{4.6}$$

and the coefficients $C_n(t_1,\ldots,t_n)$'s for n greater than or equal to 3 represent higher order correlations. For the observation times $t_1,\ldots,t_\mathcal{N}$ sufficiently away from the beginning of the integration time so that transient process may be ignored, these functions depend only on time differences. In particular, $C_1(t)$ becomes a constant and $C(t_1,t_2)$ depends only on $\tau=t_2-t_1$. In this way, we can reconcile the experimentally

defined fluorescence intensity and the autocorrelations of the preceding section.

The distribution function of the time interval Δt between two successive photon events, $\rho(\Delta t)$, referred to as Δt distribution, can also be extracted by the probability generating functional

$$\rho(\Delta t) = \frac{\text{const}}{T}\int_0^T d\tau \frac{\delta}{\delta z(\tau)}\frac{\delta}{\delta z(\tau+\Delta t)} \times \mathcal{G}[z(t)]\big|_{z(t)=1-\theta(t-\tau)\theta(\tau+\delta t-t)}, \tag{4.7}$$

where $\theta(t)=1$ for $t\leqslant 0$ and $\theta(t)=0$ otherwise, and the constant is determined by the condition

$$\int_0^T d\Delta t \rho(\Delta t) = 1. \tag{4.8}$$

We refer the reader to Appendix A for its derivation. For a Poissonian histogram, Eq. (4.7) implies $\rho(\Delta t)=\lambda e^{-\lambda \Delta t}$, as expected.

What is relevant to the actual observation is the detected photons rather than the total number of emitted ones. Let $P^{\text{eff}}_{m_1,\ldots,m_{\mathcal{N}}}$ denoted the probability of a particular histogram $\{m_1,\ldots,m_{\mathcal{N}}\}$ of detected photons. The corresponding generating function reads

$$\mathcal{G}_{\text{eff}}(z_1,\ldots,z_{\mathcal{N}}) = \sum_{m_1,\ldots,m_{\mathcal{N}}} P^{\text{eff}}_{m_1 m_2\cdots m_{\mathcal{N}}} z^{m_1}\cdots z^{m_{\mathcal{N}}}. \tag{4.9}$$

As is shown in Appendix A, under the assumption that all photon counts are statistically independent, we find a simple relation

$$\mathcal{G}_{\text{eff}}(z_1,\ldots,z_{\mathcal{N}}) = \mathcal{G}(1-\eta+\eta z_1,\ldots,1-\eta+\eta z_{\mathcal{N}}), \tag{4.10}$$

with η the efficiency of the detector. In the limit $\mathcal{N}\to\infty$, it becomes

$$\mathcal{G}_{\text{eff}}[z(t)] = \mathcal{G}[1-\eta+\eta z(t)]. \tag{4.11}$$

B. A quantum mechanical analog

The formulation we have established thus far is completely general, and independent of details of the fluorescence diffusion process. We shall now include the details of the physical process and model the generating functional $\mathcal{G}[z(t)]$. Consider N molecules, each having a specific brightness, and diffusing in a solution of total volume Ω. Both $\Omega\to\infty$ and $N\to\infty$, at a fixed concentration $c=N/\Omega$. An axially symmetric intensity profile is created by focusing the laser beam within the sample solution. While fluorescence occurs everywhere along the beam volume, the pinhole effectively eliminates the collection of photons emitted far away from the focal point [10] and a small detection volume is defined, which contains few molecules in average at all times. In the absence of chemical reactions (no self-hybridization), sufficiently weak laser intensity, and sufficiently low concentrations, we may assume that (i) N molecules do not interact with each other (except minimal collisions which maintain the equilibrium); (ii) photon emissions are statistically independent; and (iii) the photon emission frequency per fluorophore within the detection volume is $\lambda_0 u(\vec{r})$. $u(\vec{r})$ will be referred to as the fluorescence profile function and is normalized by the condition $u(0)\equiv u_{\max}(\vec{r})=1$. Under these assumptions, the probability generating functional takes the same mathematical expression of the transition matrix element of a quantum mechanical system of N noninteracting bosons in an external potential field and imaginary time, i.e.,

$$\mathcal{G}[z(t)] = \left(\frac{1}{\Omega}\right)^{\mathcal{N}}\left\langle\left|\mathcal{T}\exp\left[-\int_0^T dt H(t)\right]\right|\right\rangle, \tag{4.12}$$

where $\mathcal{T}$ enforces the time ordering and Ω is the volume of the solution and will be sent to infinity for all practical purposes. The Hamiltonian operator of the analog quantum mechanical system reads

$$H(t) = \sum_{j=1}^{N} h(\vec{r}_j,t) \tag{4.13}$$

and

$$h(\vec{r},t) = -D\nabla^2 + [1-z(t)]\lambda u(\vec{r}), \tag{4.14}$$

where D is the diffusion constant and $\lambda=k\lambda_0$ with k the effective number of fluorophores per molecule. The full derivation of Eqs. (4.12)–(4.14) is presented in Appendix B. The wave function of the state $|\rangle$ of the analog quantum mechanical system is normalized to

$$\langle \vec{r}_1,\ldots,\vec{r}_{\mathcal{N}}|\rangle = 1. \tag{4.15}$$

We notice the following.

The Hamiltonian operator (4.14) describes the motion of a particle of mass $(2D)^{-1}$ moving in an external potential $[1-z(t)]\lambda u(\vec{r})$. Two kinds of expansions can be developed for the statistical analysis. The first is a perturbative expansion according to the powers of $1-z(t)$, which generates the correlation functions to all orders. The second is the expansion according to the powers of the diffusion constant D, which is particularly useful for FCS with biological molecules. The leading order of the second expansion corresponds to the frozen limit in the literature [5,6] and we are able to add the higher order corrections systematically following this quantum mechanical analog.

It follows from Eqs. (4.11) and (4.14) that the generating functional responsible for the observed time delay histogram, $\mathcal{G}_{\text{eff}}[z(t)]$, assumes the identical mathematical form as $\mathcal{G}[z(t)]$, provided λ is replaced by $\lambda_{\text{eff}}=\eta\lambda$. In what follows, we shall refer exclusively to $\mathcal{G}_{\text{eff}}[z(t)]$ with the subscript "eff" suppressed.

The generating functional (4.12) can be factorized for each aggregate, i.e.,

$$\mathcal{G}[z(t)] = g^N[z(t)], \tag{4.16}$$

with

$$g[z(t)] = \frac{1}{\Omega}\left\langle \left| \mathcal{T} \exp\left[-\int_0^T dt h(\vec{r},t) \right] \right| \right\rangle \quad (4.17)$$

and $\langle \vec{r}| \rangle = 1$. Alternatively, $g[z(t)]$ can be calculated by integrating the wave function $\psi(\vec{r},t)$ that solves the Schrödinger equation with an imaginary time,

$$\frac{\partial}{\partial t}\psi(\vec{r},t) = -h(\vec{r},t)\psi(\vec{r},t) \quad (4.18)$$

subject to the initial condition, $\psi(\vec{r},0) = 1/\Omega$, i.e.,

$$g[z(t)] = \int d^3\vec{r}\psi(\vec{r},T). \quad (4.19)$$

To take the limit of $\Omega \to \infty$ and $N \to \infty$ at a fixed concentration c, it is crucial to notice that the difference $g[z(t)]-1$ is $O(1/\Omega)$ for a small collection volume of few molecules in average. Using the standard limit, $\lim_{N\to\infty}(1+x/N)^N = e^x$, we obtain that

$$\mathcal{G}[z(t)] = e^{-\mathcal{F}[z(t)]}, \quad (4.20)$$

with

$$\mathcal{F}[z(t)] = c\left\langle \left| 1 - \mathcal{T} \exp\left[-\int_0^T dt h(\vec{r},t) \right] \right| \right\rangle. \quad (4.21)$$

C. Generalization to multispecies and multichannels

We generalize the present formulation to include several species of fluorescent molecules with multiple channels of detection. Assuming there are M species each labeled by an index l and K detecting channels each labeled by α, the Hamiltonian of the analog quantum mechanical system, (4.13), becomes

$$H(t) = \sum_{l=1}^{M}\sum_{j=1}^{N_l} h_l(\vec{r}_j,t), \quad (4.22)$$

with

$$h_l(\vec{r},t) = -D_l\nabla^2 + \sum_{\alpha=1}^{K}[1 - z_\alpha(t)]\lambda_{l\alpha}(\vec{r}), \quad (4.23)$$

where $\lambda_{l\alpha}(\vec{r})$ the profile function specific to the lth species and αth channel. The generating functional (4.12) factorizes into a product of a single species, where each now depends on several arbitrary functions $z_\alpha(t)$. The power series expansion according to $[1-z_\alpha(t)]$'s yields all the corresponding correlation functions. Unlike number counting in the frozen limit, it can be factorized into individual detecting channels for nonzero diffusion constants.

V. ANALYTICAL EXPRESSIONS FOR DATA ANALYSIS

In this section, we shall display the analytical expressions for fluorescence intensity, the autocorrelation function, Mandel's Q parameter, and the Δt distribution, as derived from the general formulation of the preceding section. The technical details of the derivation are deferred to Appendix C.

A. Fluorescence intensity, correlation functions, and the binning statistics

In accordance with Eqs. (4.4) and (4.5), the ensemble average of the fluorescence intensity reads

$$I = c\lambda \int d^3\vec{r}u(\vec{r}) = n\lambda, \quad (5.1)$$

where $n = cv$ with $v \equiv \int d^3\vec{r}u(\vec{r})$. The integration v can be viewed as the effective collection volume defined by the focused beam and pinhole and n, the average number of molecules within the volume. The experiments reported in this paper are characterized by $n \sim 1$.

Applying the definition (4.4) and the quantum mechanical analog (4.12)–(4.14) of $\mathcal{G}[z(t)]$, the second-order correlation $C_2(t_1,t_2)$ takes the form

$$C_2(t_1,t_2) = c\lambda^2 \int \frac{d^3\vec{p}}{(2\pi)^3} u_{\vec{p}}^2 e^{-|t_1-t_2|Dp^2}, \quad (5.2)$$

with $u_{\vec{p}} = \int d^3\vec{r}e^{-i\vec{p}\cdot\vec{r}}u(\vec{r})$ the Fourier transformation of the profile function $u(\vec{r})$. Substituting Eqs. (5.1) and (5.2) into Eq. (4.6) for the autocorrelation function, we find the following.

For an arbitrary $u(\vec{r})$, the autocorrelation function at zero time lag takes a simple form

$$A(0) = \frac{Z}{n}, \quad (5.3)$$

with Z the geometrical factor given by

$$Z = \frac{\int d^3\vec{r}u^2(\vec{r})}{\int d^3\vec{r}u(\vec{r})}. \quad (5.4)$$

For nonzero time lag, we shall parametrize the autocorrelation function as

$$A(\tau) = \frac{Z}{n}\mathcal{A}(\tau), \quad (5.5)$$

with $\mathcal{A}(0) = 1$.

For a three-dimensional Gaussian fluorescence profile,

$$u(\vec{r}) = e^{-(x^2+y^2)/2\omega_\perp^2 - z^2/2\omega_\parallel^2}, \quad (5.6)$$

we obtain that $Z = 1/2\sqrt{2}$ and [1]

$$\mathcal{A}(\tau) = \frac{1}{\left(1+\frac{\tau}{\tau_\perp}\right)\sqrt{1+\frac{\tau}{\tau_\parallel}}}, \quad (5.7)$$

with $\tau_\perp = \omega_\perp^2/D$ and $\tau_\parallel = \omega_\parallel^2/D$. For a Gaussian-Lorentzian profile,

$$u(\vec{r}) = \frac{\omega_\parallel^2}{\omega_\parallel^2 + z^2} e^{-(x^2+y^2)/2\omega_\perp^2}, \tag{5.8}$$

we find that $Z=\frac{1}{4}$ and

$$\mathcal{A}(\tau) = \frac{2}{\left(1+\frac{\tau}{\tau_\perp}\right)} \sqrt{\frac{\tau_\parallel}{\tau}} e^{\tau/\tau_\parallel} \mathrm{erfc}\left(\sqrt{\frac{\tau_\parallel}{\tau}}\right), \tag{5.9}$$

with

$$\mathrm{erfc}(z) = \int_z^\infty dx e^{-x^2} = \frac{e^{z^2}}{2z}\left[1 - \frac{1}{2z^2} + O(z^{-4})\right]. \tag{5.10}$$

For $\tau \ll \tau_\parallel$ and $\tau_\perp \ll \tau_\parallel$, both Eqs. (5.7) and (5.9) can be approximated by

$$\mathcal{A}(\tau) = \frac{1}{1+\frac{\tau}{\tau_\perp}}. \tag{5.11}$$

Extending the same analysis to the third-order coefficient of the expansion of $\ln \mathcal{G}$ according to the power of $z(t)-1$, we find the third-order correlation function for $\tau_\perp \ll \tau_\parallel$, i.e.,

$$C_3(t_1,t_2,t_3) = \frac{Z'}{\left(1+\frac{\tau}{\tau_\perp}\right)\left(1+\frac{\tau'}{\tau_\perp}\right) - \frac{1}{4}}, \tag{5.12}$$

where the constant Z' is another geometrical factor, such as Z for the autocorrelation, $\tau \equiv t_a - t_b$, $\tau' \equiv t_b - t_c$ with t_a, t_b, and t_c a permutation of t_1, t_2, and t_3 such that $t_a > t_b > t_c$.

Using Eq. (2.6), we obtain the expression of the Q parameter which agrees with that of FIMDA [11]. For $\tau \ll \tau_\parallel$ it can be approximated by

$$\delta = 2Z\lambda\tau_\perp\left(\frac{\tau+\tau_\perp}{\tau}\ln\frac{\tau+\tau_\perp}{\tau_\perp} - 1\right), \tag{5.13}$$

with the dependence on different models of longitudinal profile absorbed in the constant Z.

The distribution of photon counting numbers within a time bin can be extracted from the generating function $G(z)$, obtained from the generating functional $\mathcal{G}(z)$ by restricting the form of $z(t)$ such that it equals to a constant z within the time bin and vanishes elsewhere. We then have

$$G(z) = e^{-nF(\tau|1-z)}, \tag{5.14}$$

with

$$F(\tau|\zeta) \equiv \frac{c}{n}\langle|1 - e^{-\tau h(\zeta)}|\rangle \tag{5.15}$$

and

$$h(\zeta) = -D\nabla^2 + \zeta\lambda u(\vec{r}). \tag{5.16}$$

While an analytical expression for $F(\tau|\zeta)$ does not exist in general, the expansion according to diffusion constant can be obtained easily,

$$F(\tau|\zeta) = \zeta\lambda\tau f(\zeta\lambda\tau) - \frac{1}{3\lambda\tau_\perp}\zeta^2\lambda^2\tau^3 f'(\zeta\lambda\tau) + O\left(\frac{1}{\lambda^2\tau_\perp^2}\right), \tag{5.17}$$

with

$$f(x) = \frac{4}{3\sqrt{\pi}}\int_0^1 d\xi \ln^{3/2}\frac{1}{\xi} e^{-x\xi}, \tag{5.18}$$

where the leading term corresponds to the frozen limit in Ref. [11] and the second term improves the approximation further.

B. The time delay histogram

Carrying out the functional derivatives in the formulas (4.7) with the aid of Eqs. (4.16) and (4.17), the distribution function $\rho(\Delta t)$ becomes

$$\begin{aligned}\rho(\Delta t) &= \frac{1}{\lambda n}\frac{d^2}{d\Delta t^2} e^{-nF(\Delta t|1)} \\ &= \lambda\left[-\frac{\partial^2 F}{\partial(\lambda\Delta t)^2} + n\left(\frac{\partial F}{\partial(\lambda\Delta t)}\right)^2\right] \\ &\quad \times e^{-nF(\Delta t|1)}.\end{aligned} \tag{5.19}$$

Using expansion (5.17), we derive an approximate expression of $\rho(\Delta t)$ which is valid for $\lambda\tau_\perp \gg 1$ and $\Delta t \ll \tau_\perp$,

$$\begin{aligned}\ln\rho(\Delta t) &= \ln\rho(0) - nxf(x) + \ln\left\{[f(x)+xf'(x)]^2 - \frac{1}{n}[2f'(x)+xf''(x)]\right\} \\ &\quad + \frac{1}{\lambda\tau_\perp}\left\{-\frac{1}{3}nx^3 f'(x) + \frac{2xf'(x) + 2x^2 f''(x) + \frac{1}{3}x^3 f'''(x) - 2nx^3[f(x)+xf'(x)]\left[f'(x) - \frac{1}{3}xf''(x)\right]}{-2f'(x) - xf''(x) + n[f(x)+xf'(x)]^2}\right\},\end{aligned} \tag{5.20}$$

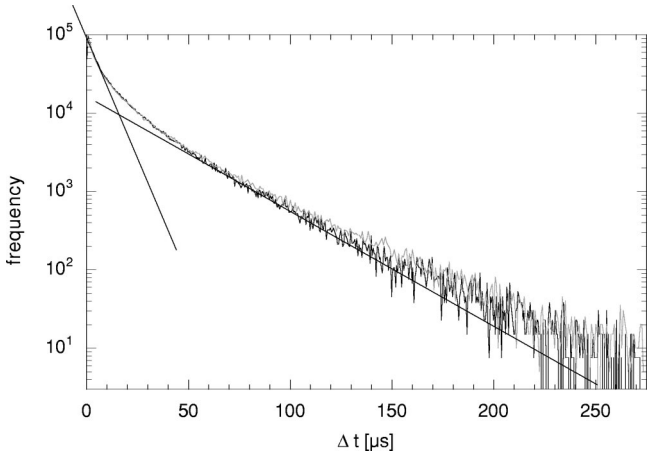

FIG. 3. The time delay histograms for single (black) and double (gray) labeled ssDNA. The resulting distributions from a single Poisson processes are shown by the straight lines for comparison.

with $x=\lambda\Delta t$. Alternatively, a Taylor expansion of F in $\lambda\Delta t$ yields an expression of $\rho(\Delta t)$ for $\lambda\Delta t \ll 1$.

For Taylor expansion of the function F according to the power of Δt, we obtain

$$\ln \rho(\Delta t) = \ln \rho(0) - (n+\gamma)\lambda\Delta t + \tfrac{1}{2}(\beta-\gamma^2)\lambda^2\Delta t^2 + O(\Delta t^3), \tag{5.21}$$

where

$$\gamma = \frac{3^{-3/2} + 2^{-1/2}n + \dfrac{2^{-3/2}}{\lambda\tau_\perp}}{2^{-3/2}+n}$$

and

$$\beta = (2^{-3/2}+n)^{-1}\left[\frac{1}{8} + \left(\frac{3}{8} + 2\cdot 3^{-3/2}\right)n + 2^{-3/2}n^2 + \frac{4\cdot 3^{-5/2} + 2^{-1/2}n}{\lambda\tau_\perp}\right]. \tag{5.22}$$

If the histogram were a Poissonian, a single exponential would be expected, which corresponds to $\beta=\gamma=0$. The parameters β and γ represent the deviation from a Poissonian which do not vanish even in the frozen limit, i.e., $\tau_\perp \to \infty$ and $\tau_\parallel \to \infty$.

VI. RESULTS

Photon counting data were collected for two systems, and the time delay histogram constructed for each (Fig. 3). Both samples consist of very dilute (nanomolar) identical sequences of ssDNA in buffer, and observations were made at room temperature (25 °C). We consider these systems noninteracting. In the first sample, specifically single end-labeled ssDNA was diluted to an average concentration of 1 molecule per collection beam volume at any time. The number of molecules was calculated from calibration of the collection volume (see Methods) at 100 μW incident power (0.35 μm^3). The second sample contained the same sequence ssDNA, however, tagged with two fluorophores per object (one at each end). This sample was then diluted so that the average intensity in time of the two samples were *equal*. If the dimer system was exactly twice the fluorescence of the monomer, then the dimer concentration should be 0.5 that of the monomer for the same given intensity. However, due to local quenching effects of the fluorophore, the average concentration of double-dyed molecules in the beam at any time was calculated to be 0.7 to maintain the same intensity. The empirical volume of the beam was calibrated from a serial dilution of a standard dye solution, and the rate of emitted photons per fluor, λ, measured: $1/\lambda = 1/60$ kHz. Concentrations of single/double fluorescent aggregates in the beam were 1 and 0.7 molecules, respectively.

Empirical measurements demonstrated the quenching could be minimized by hybridization of the ssDNA to a nonfluorescent target. Hybridization of such a short segment (below the persistent length of dsDNA) forces the two fluorophores farther apart, minimizing dye-dye interaction. However, double-dyed molecules never demonstrated a full factor of 2 increase in fluorescence over their single-dyed counterparts. We suspect local quenching interaction of the fluor with the nearby base of the target strand.

The characteristic diffusion time through the sampling volume was extracted from the decay of the autocorrelation function. Due to the resolution of our correlator software (10^{-8} s -10^{-2} s), we are most sensitive to the diffusion across the short axis of the beam profile. Hence, the characteristic time extracted from time correlation of the data is most representative of $\tau_\perp$. Through FCS measurements, we find that $\tau_\perp \simeq 300$ μs for both single-dyed molecules and double-dyed molecules. Using a random walk simulation and a geometrical approximation for the long axis of the beam profile, we estimate $\tau_\parallel$ to be $100\tau_\perp$.

In all theoretical curves of the figures below, we use $\lambda = 60$ kHz for specific brightness of the single-dyed molecules and an enhancement of $1/0.7 \simeq 1.4$ for the double-dyed molecules. The transverse diffusion time $\tau_\perp = 300$ μs is substituted into the theoretical formula for both single-dyed and double-dyed molecules.

At first glance, the two distributions of Fig. 3 are completely indistinguishable. However upon closer examination it is possible to see the two curves slowly diverge at large Δt with the double-dye data falls slightly above the single-dye data. The comparison between the analytical expression of the time delay histograms with large and small Δt approximations (5.20) and (5.21) is shown in Fig. 4, where the ratio of the experimental histogram to the theoretical one is plotted versus the time delay Δt. It is evident that the formula (5.19) together with the approximation (5.17), denoted as $\rho_{\text{theory}}(\Delta t)$ in the figures, is robust for single- (a) and double-dyed (c) samples. (b) and (d) are exploded views of the small Δt domain of each histogram. The curve labeled by "linear" or "quadratic" corresponds to the theoretical formula (5.21) with terms beyond linear or quadratic truncated. The quality of the agreement is improved from the linear truncation to

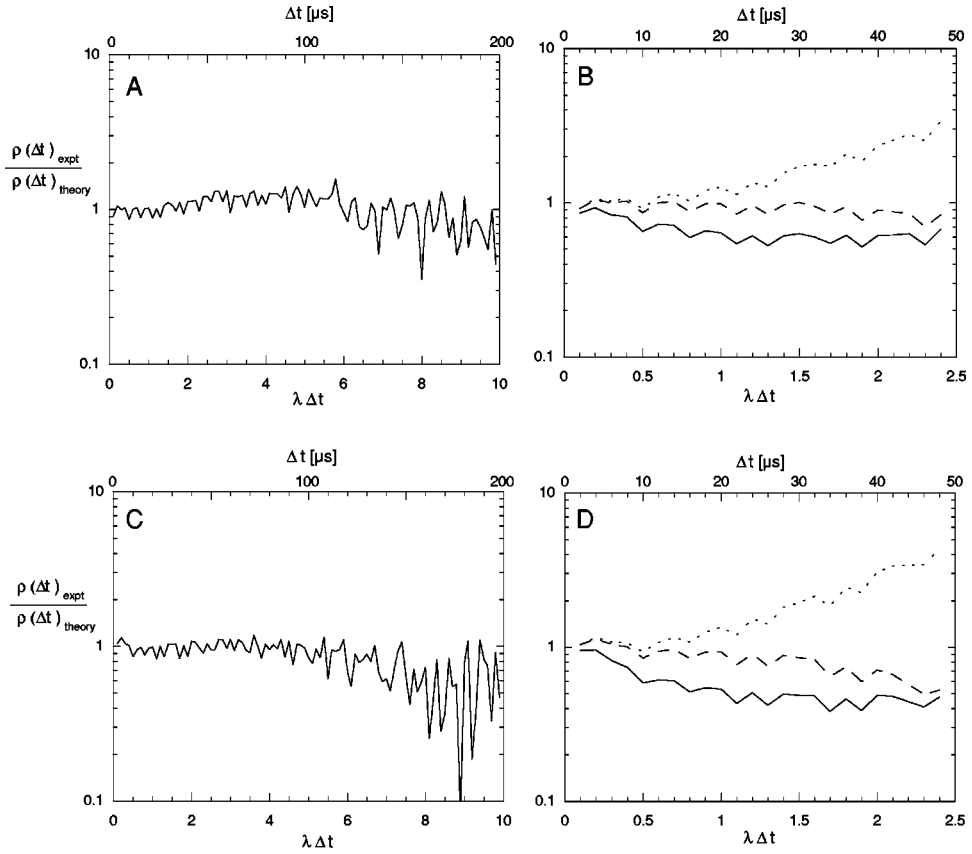

FIG. 4. (a) large $\triangle t$ single fluor, (b) small $\triangle t$ single fluor, (c) large $\triangle t$ double fluor, and (d) and small $\triangle t$ double fluor. (Solid) Poisson, (short dash) linear, and (long dash) quadratic fits are shown for comparison in the short time limits.

the quadratic truncation. The curve labeled by "Poisson" corresponds to $\rho_{\text{theor}}(\Delta t)$ given by a Poissonian, i.e., $\ln \rho_{\text{theor}}(\Delta t) = \ln \rho_{\text{theor}}(0) - \lambda \Delta t$, which is clearly a poor description of the experimental histogram.

Although these simulations successfully differentiate the two systems, the analysis is somewhat cumbersome. A common mathematical technique to highlight the subtle differences in distributions is moment analysis. Similar techniques have proven useful in fluctuation spectroscopy [13–15]. The first moment is the mean, the second moment the standard deviation, the third the skewness, etc.

Returning to Fig. 3, we note a profound difference between the experimental data and a single Poissonian process. The straight lines represent two hypothetical single Poission systems with different time scales. For the simple detection of emitted photons within a fixed volume one might expect the statistics to resemble a single Poissonian process [16]. However, when the particles are allowed to diffuse through the boundaries of the volume, an additional Poissonian process contributes to the overall photon statistics [17,18]. Not only must we account for the stochastic nature of the emission process, we must also consider the number distribution of aggregates passing into the beam volume from the larger sample reservoir.

The statistics of the time series of the photon counting can be highlighted through Mandel's Q parameter [Eq. (2.5)] introduced in Sec. II. We develop the binning moment as a complementary technique to FIMDA. In FIMDA [9] each histogram is representative of the number count distribution using a certain binning window size. For every change in binning window size, a new histogram is constructed. Likewise, every histogram has its own unique set of moments. All first moments should be equal to the product of the average intensity and the window size will not show any difference between the two systems (single dye and double dye) in accordance with the experimental procedure described in the first paragraph of this section. Starting with the second moment, the difference between the two systems emerges. In Fig. 5, we plot the second moment normalized according to Eq. (2.5) for both system and the corresponding theoretical curve given by Eq. (5.13). The data for the two systems are clearly distinguishable and agree well with the theoretical prediction.

If the photon histogram were a single Poissonian, all correlations as well as the Q parameter would vanish. Therefore the correlation functions and the Q parameter measure the deviation of the photon histogram from a Poissonian. Recall that the time delay histogram is essentially the result of two Poissonian processes. If we reexamine Fig. 3 (although it is a time delay, not number counting histogram) and focus on the dashed line through the short Δt domain, divergence from the single Poisson increases as Δt increases. For binning windows smaller than the diffusion time, the statistics are primarily due to the intrinsic fluorescence of the fluorophore. Since both systems contain two fluors, the two distributions vary little in this domain. At longer times, each molecule samples the inhomogeneous beam profile as it diffuses.

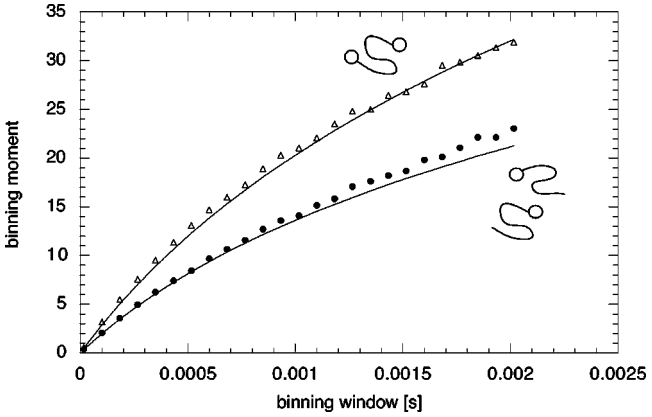

FIG. 5. Q parameters of (•) single-dye and (△) double-dyed aggregates. A cartoon of each system is displayed next to the corresponding curve.

Hence the diffusion dependent statistics dominate the long time domain and are responsible for the notably different Q parameters of the samples.

VII. SECONDARY EFFECTS

In traditional fluorescence correlation spectroscopy, triplet state effects and various quenching processes are the principal mechanisms that overshadow structural information. To parse out these contributions, one may need to explore the higher binning moments that have not been examined in this work. Our mathematical formulation provides the complete systematics for this purpose. Such secondary effects introduce additional time scales to the problem (not simply the fluorescence rate and the diffusion time to cross the collection volume discussed in this paper). Also, some details of the electronic transition inside a fluorophore should be addressed. This modeling can be achieved by enlarging the quantum mechanical analog with a multicomponent wave function ψ_i and a matrix Hamiltonian

$$h_{ij} = -D\nabla^2\delta_{ij} + V_{ij}, \tag{7.1}$$

where

$$V_{ij} = \begin{cases} z(t)W_{ij} & \text{if } i \to j \text{ is a fluorescence transition} \\ \mathrm{W}_{ij} & \text{if } i \to j \text{ is not a fluorescence transition} \\ -\sum_k W_{ik} & \text{if } i = j. \end{cases} \tag{7.2}$$

Each component of the wave function, ψ_i, represents the probability of a DNA molecule at a particular spatial location with its fluorophore in the ith electronic level and W_{ij} the transition rates from ith$\to j$th of electronic levels.

In principle, such an elaboration should also be implemented in the absence of triplet state effects and quenching processes, since the fluorescence rate combines the excitation rate from the ground state and the spontaneous emission rate from the excitation levels. For two electronic levels with "0" labeling the ground state and "1" the excitation state, we have $W_{01}=\lambda u(\vec{r})$ and $W_{10}=\lambda_s$, Einstein's A coefficient. The Schrödinger equation (4.18) is split into two components:

$$\frac{\partial}{\partial t}\psi_0 = (D\nabla^2 - \lambda u)\psi_0 + z(t)\lambda_s\psi_1, \tag{7.3}$$

$$\frac{\partial}{\partial t}\psi_1 = (D\nabla^2 + \lambda_s u)\psi_1 - \lambda u\psi_0. \tag{7.4}$$

The approximation employed in previous sections amounts to $\lambda_s \gg \lambda$ and $\lambda \gg 1/\tau_\perp$, the inverse diffusion time. In this case, the spontaneous emission is almost instantaneous once the fluorophore is excited and the second equation, (7.4), gives rise to $\lambda_s\psi_1 \simeq \lambda u\psi_0$ at equilibrium. Substituting it back (7.3), we obtain Eq. (4.18) with h given by Eq. (4.14). For the experimental data presented in this paper, a 60 kHz photon time delay histogram at 3 % detection efficiency, the excitation rate is $60/3\ \% = 2$ MHz, and the corresponding fluorescence time is 500 ns, much longer than the typical spontaneous emission time, 10 ns. Our approximation is therefore adequate.

VIII. CONCLUDING REMARKS

We have developed a mathematical formulation to analyze the time delay series of fluorescence photons from diffusing particles, based on a probability generating functional and its quantum mechanical analog. Although it may appear formal, since some analytical expressions such as the autocorrelation function have been obtained by less sophisticated means, the approach is systematic. The potential of this general approach will be realized when dealing with systems of greater complexity.

We have designed an experiment to differentiate fluorescent aggregates in solution. ssDNA monomers are labeled with a single fluorophore and dimers with two fluorophores. Secondary effects such as chemical reactions, triplet state effects, and various quenching processes have been neglected in our model. However these effects have been minimized by using dilute solutions to avoid self-interaction and Rhodamine 6G, a fluorophore with little triplet state at low incident intensities.

Although we have only addressed ideal experimental conditions of the nonreacting case in this paper, typical biological/chemical systems react (aggregation or cooperative binding). Our technique can be modified to include these reactions. One must generalize the quantum mechanical analog to the case with several species of particles, each representing a fluorescence molecule, interacting with each other. Without going to technical details which will be reported elsewhere, we quote the generalization of our formulation analog in the presence of a binary reaction,

$$2A \Leftrightarrow B. \tag{8.1}$$

The Hamiltonian of the quantum mechanical analog in Eq. (4.12) is given by

$$H = H_{\mathrm{diff}} + H_{\mathrm{fluor}} + H_{\mathrm{chem}}, \tag{8.2}$$

where

$$H_{\text{diff}} = \int d^3r (D_A \vec{\nabla}\overline{\psi}\cdot\vec{\nabla}\psi + D_B \vec{\nabla}\overline{\phi}\cdot\vec{\nabla}\phi), \tag{8.3}$$

$$H_{\text{fluor}} = [1 - z(t)] \int d^3r u(\vec{r})[(\lambda_A \overline{\psi}\psi + \lambda_B \overline{\phi}\phi), \tag{8.4}$$

and

$$\begin{aligned} H_{\text{chem}} = &-\frac{1}{2}\int d^3r \int d^3r' \int d^3\vec{R}\sigma(\vec{R}|\vec{r},\vec{r}')\overline{\phi}(\vec{R})\psi(\vec{r})\psi(\vec{r}') \\ &-\frac{1}{2}\int d^3r \int d^3r' \int d^3\vec{R}\sigma'(\vec{r},\vec{r}'|\vec{R})\overline{\psi}(\vec{r})\overline{\psi}(\vec{r}')\phi(\vec{R}) \\ &+\frac{1}{2}\int d^3r \int d^3r' \int d^3\vec{R}\sigma(\vec{R}|\vec{r},\vec{r}')\overline{\psi}(\vec{r}')\overline{\psi}(\vec{r})\psi(\vec{r})\psi(\vec{r}') \\ &+\frac{1}{2}\int d^3r \int d^3r' \int d^3\vec{R}\sigma'(\vec{r},\vec{r}'|\vec{R})\overline{\phi}(\vec{R})\phi(\vec{R}), \end{aligned} \tag{8.5}$$

and the generating functional is no longer factorizable. In this Hamiltonian, the pairs of operators $(\psi,\overline{\psi})$ or $(\phi,\overline{\phi})$ are the creation/annihilation operators of a molecule of species A or B. $D_{A(B)}$ and $\lambda_{A(B)}$ are the diffusion constant and the specific brightness of the species $A(B)$. The first term of the reaction part, H_{chem}, represents the creation of a B molecule, the second term represents the creation of a pair of A molecules, the third term signifies the annihilation of a pair of A molecules, and the last term signifies the annihilation of a B molecule. The function $\sigma(\vec{R}|\vec{r},\vec{r}')$ or $\sigma'(\vec{r},\vec{r}'|\vec{R})$ denotes the reaction rate in each direction of Eq. (8.1). In physics, the Hamiltonian (8.2) describes a system of interacting bosons of two species. The equilibrium state of the fluorescence-diffusion-reaction process will be analogous to the ground state which carries a Bose condensate. The proportion of each species in the condensate is determined by the mass-action law and the fluctuations are calculable with well developed field theoretic method. In terms of the generating functional (4.12) and the functional derivative (4.4), we are able to calculate various correlation functions of the photon counting histogram in the presence of chemical reactions using techniques developed in quantum field theory. This approach is expected to be more systematic than the conventional reaction kinetics.

ACKNOWLEDGMENTS

The works of N.L. Goddard, G. Bonnet, and A. Libchaber are supported in part by Mathers Foundation and the Burrough-Welcome Fund. The work of H.C.R. was supported in part by U.S. Department of Energy under the Contract No. DE-FG02-91ER40651-TASK B. We would also like to thank David Mauzerall for discussions and suggestions.

APPENDIX A

1. The derivation of the formulas for distribution function of the time-delay histogram

To derive the Δt distribution (the distribution function of the time interval between two successive photon emissions), we start with the case with finite time bins (ϵ is sufficiently small that the probability of more than one photons within a bin can be ignored) and look for the probability of one photon event in nth bin, one photon event in $(n+l)$th bin with $\Delta t=(l-1)\epsilon$, and no photon in the bins between them. Up to a normalization constant, the probability is

$$\begin{aligned} \rho_{nl} &= \text{const} \sum_{m_1,\ldots,m_{n-1},m_{n+l+1},\ldots,m_{\mathcal{N}}} P_{m_1\cdots m_{n-1}10\cdots 01 m_{n+l+1}\cdots m_{\mathcal{N}}} \\ &= \frac{\partial}{\partial z_n}\frac{\partial}{\partial z_{n+l}}\mathcal{G}(1,\ldots,1,z_n,0,\ldots,0,z_{n+l},1,\ldots,1). \end{aligned} \tag{A1}$$

By summing over n with a fixed l, we find the probability of successive $l-1$ empty bins

$$\rho_l = \sum_n \rho_{nl}. \tag{A2}$$

Taking the limit of infinitesimal bins, i.e., $\epsilon\to 0$ at fixed T and Δt, we obtain the desired distribution function (4.7).

2. Detector effect

Consider the case of a single time bin, i.e., $\mathcal{N}=1$, we have

$$\mathcal{G}(z) = \sum_{m=0}^{\infty} P_m z^m \tag{A3}$$

and

$$\mathcal{G}_{\text{eff}}(z) = \sum_{m=0}^{\infty} P_m^{\text{eff}} z^m. \tag{A4}$$

Under the assumption that each photon counting by the detector is statistically independent of others, the probability of detecting m photons out of n incident photons is

$$\frac{n!}{m!\,(n-m)!}\eta^m(1-\eta)^{n-m}, \tag{A5}$$

with η the detector efficiency. Therefore

$$P_m^{\text{eff}} = \sum_{n=m}^{\infty} P_n \frac{n!}{m!\,(n-m)!}\eta^m(1-\eta)^{n-m}. \tag{A6}$$

Substituting Eq. (A6) into Eq. (A4), we obtain that

$$\mathcal{G}_{\text{eff}}(z) = \sum_{m=0}^{\infty}\sum_{n=m}^{\infty} P_n \frac{n!}{m!\,(n-m)!}\eta^m(1-\eta)^{n-m}z^m$$
$$= \sum_{n=0}^{\infty} P_n \sum_{m=0}^{n} \frac{n!}{m!\,(n-m)!}(\eta z)^m(1-\eta)^{n-m}$$
$$= \sum_{n=0}^{\infty} P_n(1-\eta+\eta z)^n$$
$$= \mathcal{G}(1-\eta+\eta z). \tag{A7}$$

Following the same steps for each variable in the case with $\mathcal{N}>1$, we end up with Eqs. (4.10) and (4.11).

APPENDIX B

The probability generating functional of the photon emission histogram from N identical fluorescence molecules is modeled according to the following two principles.

The generating functional with N nonreacting molecules,

$$\mathcal{G}[z(t)] = g^N[z(t)], \tag{B1}$$

with $g[z(t)]$ the generating functional of one molecule.

The generating functional of one molecule,

$$g[z(t)] = \sum_{\mathcal{C}} P_{\mathcal{C}} g_{\mathcal{C}}[z(t)], \tag{B2}$$

where $g_{\mathcal{C}}[z(t)]$ denote the generating functional along a particular diffusion path $\mathcal{C}$ and $P_{\mathcal{C}}$ the probability of the path.

Dividing the integrating time T into $\mathcal{N}$ time bins with $t_0=0,\ldots,t_n=n\epsilon,\ldots,t_{\mathcal{N}}=\mathcal{N}\epsilon=T$ and specifying a diffusion path $\mathcal{C}$ by the location of the molecule at each instant, $(t_0,\ldots,t_n,\ldots,T)$, i.e.,

$$\mathcal{C} = \{\vec{r}_0,\ldots,\vec{r}_n,\ldots,\vec{r}_{\mathcal{N}}\}. \tag{B3}$$

For sufficiently small ϵ, the probability of more than one photon in each bin may be ignored and we have

$$g_{\mathcal{C}}[z(t)] = \lim_{\epsilon\to 0}\prod_{n=0}^{\mathcal{N}-1}[1-\epsilon\lambda u(\vec{r}_n)+\epsilon\lambda z_n u(\vec{r}_n)]$$
$$= \lim_{\epsilon\to 0}\exp\left[\lambda\epsilon\sum_{n=0}^{\mathcal{N}-1}(z_n-1)u(\vec{r}_n)\right]. \tag{B4}$$

The probability of the path $\mathcal{C}$ is entirely determined by diffusion. Since the probability for a molecule to diffuse from $\vec{r}_n$ at t_n to $\vec{r}_{n+1}$ at t_{n+1} is

$$\left(\frac{1}{4\pi D\epsilon}\right)^{3/2} d^3\vec{r}_{n+1} e^{-(\vec{r}_{n+1}-\vec{r}_n)^2/4D\epsilon}, \tag{B5}$$

$$P_{\mathcal{C}} = \prod_{n=0}^{\mathcal{N}-1}\left(\frac{1}{4\pi D\epsilon}\right)^{3/2} d^3\vec{r}_{n+1} e^{-(\vec{r}_{n+1}-\vec{r}_n)^2/4D\epsilon}. \tag{B6}$$

It follows from Eqs. (B2), (B4), and (B6) that

$$g[z(t)] = \frac{1}{\Omega}\lim_{\mathcal{N}\to\infty}\left(\frac{1}{4D\pi\epsilon}\right)^{3\mathcal{N}/2}\int\prod_{n=0}^{\mathcal{N}} d^3\vec{r}_n \exp[-\epsilon\sum_n L_n], \tag{B7}$$

with

$$L_n = \frac{1}{4D}\left(\frac{\vec{r}_{n+1}-\vec{r}_n}{\epsilon}\right)^2 + (1-z_n)\lambda u(\vec{r}_n), \tag{B8}$$

where we have taken the average of the initial location of the molecule, $\vec{r}_0$, over the volume of the solution. Mathematically, Eqs. (B7) and (B8) present a path integral of a quantum mechanical particle moving in an external potential $[1-z(t)]\lambda u(\vec{r})$ in an imaginary time. A similar path integral has been used to describe fluorescence correlations [19]. Following the standard procedure [20], we may cast Eq. (B7) into the canonical form

$$g[z(t)] = \frac{1}{\Omega}\left\langle\left|\mathcal{T}\exp\left[-\int_0^T dt h(t)\right]\right|\right\rangle, \tag{B9}$$

where $\mathcal{T}$ is the time ordering operator,

$$h(t) = -D\nabla^2 + [1-z(t)]\lambda u(\vec{r}) \tag{B10}$$

is the analog of the quantum mechanical Hamiltonian operator and $|0)$ is the analog of a quantum mechanical state, whose wave function is $\langle\vec{r}|\rangle=1$.

Finally, we would like to explain the operator $\mathcal{T}$ in more detail, when acting on a product of operator functions of time, it arranges the order of these operators according to the descending order of their time arguments, i.e.,

$$\mathcal{T}O(t_1)O(t_2)\cdots O(t_n) = O(t_{P_1})O(t_{P_2})\cdots O(t_{P_n}), \tag{B11}$$

with $P_1,P_2,\ldots,P_n$ a permutation of $1,2,\ldots,n$, such that $t_{P_1}\geqslant t_{P_2}\geqslant\cdots\geqslant t_{P_n}$. This property, when applied to the Taylor expansion of the exponential operator in Eq. (B9), yields

$$\mathcal{T}\exp[-\int_0^T dt h(t)]$$
$$= 1-\int_0^T dt h(t)+\int_0^T dt_2\int_0^{t_2} dt_1 h(t_2)h(t_1)$$
$$+\cdots+(-)^n\int_0^T dt_n\int_0^{t_n} dt_{n-1}\cdots\int_0^{t_2} dt_1 h(t_n)$$
$$\times h(t_{n-1})\cdots h(t_1)+\cdots. \tag{B12}$$

APPENDIX C

For a time independent operator A and a time dependent operator $B(t)$, the following identity holds with the time ordering product:

$$\mathcal{T}\exp\left[-\int_0^t d\tau[A+B(\tau)]\right] = e^{-tA}\left[\mathcal{T}\exp\left\{-\int_0^T d\tau\mathcal{B}(\tau)\right\}\right], \tag{C1}$$

with $\mathcal{B}(\tau)=e^{\tau A}B(\tau)e^{-\tau A}$.

The expansion of the functional (4.21) that generates all correlation coefficients for a nonreacting system follows from the identity (C1) with $A=-D\nabla^2$ and $B=[1-z(t)]\lambda u(\vec{r})$. We find

$$\mathcal{F}[z(t)] = \mathcal{C}[\int_0^T dt[1-z(t)]\langle|u|\rangle - \int_0^T dt_2[1-z(t_2)] \times \int_0^t 2dt_1[1-z(t_1)]\langle|ue^{(t_2-t_1)D\nabla^2}u|\rangle + \cdots], \tag{C2}$$

$$I = C_1(t) = c\lambda\langle|u|\rangle, \tag{C3}$$

and

$$C_2(t,t') = c\lambda^2\langle|ue^{|t-t'|D\nabla^2}u|\rangle. \tag{C4}$$

This expansion is parallel to the perturbative expansion of the quantum mechanical analog.

The expansion in the diffusion constant for a nonreacting system is obtained by applying the identity (C1) with $A=-\lambda u$, $B=-D\nabla^2$, and $t=\Delta t$, and making a Taylor expansion of the second factor on the right-hand side of Eq. (C1):

$$nF(\tau|\zeta) = \mathcal{C}\left[\langle|1-e^{-\zeta\lambda\tau u}|\rangle - \int_0^\tau ds\langle|e^{-\zeta\lambda(\tau-s)u}D\nabla^2e^{-s\zeta\lambda\tau u}|\rangle + \cdots\right]. \tag{C5}$$

This expansion corresponds to the strong coupling expansion of the quantum mechanical analog.

The calculation of the expectation value $\langle|\cdots|\rangle$ in Eqs. (C2) and (C5) is facilitated by switching between the coordinate and momentum representations of the quantum mechanical analog. The state $|\rangle$ is the state of zero momentum and is normalized the volume of the system.

[1] D. Magde, E. L. Elson, and W. W. Webb, Phys. Rev. Lett. **29**, 704 (1972).
[2] G. Bonnet, O. Krichevsky, and A. Libchaber, Proc. Natl. Acad. Sci. U.S.A. **95**, 8602 (1998).
[3] E. L. Elson and D. Magde, Biopolymers **13**, 1 (1974).
[4] C. R. Cantor and P. R. Schimmel, Biophysical Chemistry: Techniques for the Study of Structure and Function, 1980, Vol. II (unpublished).
[5] Y. Chen, J. D. Müller, P. T. C. So, and E. Gratton, Biophys. J. **77**, 553 (1999).
[6] P. Kask, K. Palo, D. Ulmann, and K. Gall, Proc. Natl. Acad. Sci. U.S.A. **96**, 13 756 (1999).
[7] E. Novikov and N. Boens, J. Chem. Phys. **114**, 1745 (2001).
[8] P. Schwille, F. J. Meyer-Almes, and R. Rigler, Biophys. J. **72**, 1878 (1997).
[9] K. Palo, Ü. Mets, S. Jäger, P. Kask, and K. Gall, Biophys. J. **79**, 2858 (2000).
[10] R. Rigler, U. Mets, J. Widengren, and P. Kask, Eur. Biophys. J. **22**, 69 (1993).
[11] P. Kask, K. Palo, N. Fay, L. Brand, Ü. Mets, D. Ullmann, J. Jungmann, J. Pschorr, and K. Gall, Biophys. J. **78**, 1703 (2000).
[12] L. Mandel, Opt. Lett. **4**, 205 (1979).
[13] A. G. Palmer and N. L. Thompson, Biophys. J. **52**, 257 (1987).
[14] H. Qian and E. L. Elson, Proc. Natl. Acad. Sci. U.S.A. **87**, 5479 (1990).
[15] H. Qian and E. L. Elson, Biophys. J. **57**, 374 (1990).
[16] L. Mandel, Proc. Phys. Soc. **72**, 1037 (1958).
[17] D. L. Snyder, *Random Point Processes* (Wiley-Interscience, New York, 1975).
[18] L. Mandel and E. Wolf, *Optical Coherence and Quantum Optics* (Cambridge University Press, Cambridge, 1995).
[19] J. Enderlein, Phys. Lett. **6**, 427 (1996).
[20] R. P. Feynman and A. Q. Hibbs, *Quantum Mechanics and Path Integrals* (McGraw-Hill, New York, 1965).